Vapor−Liquid Equilibrium Data and Predictive Correlations for the Carbon Dioxide−Dimethyl Carbonate Binary Mixture

Rocco P. Ciccolini, Adam C. Madlinger, Sean A. Rogers, and Jefferson W. Tester*

Chemical Engineering Department, Massachusetts Institute of Technology, 77 Massachusetts Avenue, Cambridge, Massachusetts 02139

Mixture critical points and liquid-phase density, component concentration, and volume expansion were measured for the carbon dioxide−dimethyl carbonate binary mixture at temperatures between (310 and 423) K [(37 to 150) °C] and pressures between (1.1 and 14.4) MPa. Data were correlated well by the Redlich−Kwong−Aspen equation of state as well as several empirical engineering correlations. Importantly, the experimental and modeling procedures outlined in this work may be adapted to other carbon dioxide−liquid binary mixtures and used to facilitate the design of CO_2-based reaction and separation processes.

Introduction

For more than twenty years, carbon dioxide (CO_2) in a liquid and supercritical state has attracted considerable attention as an "environmentally friendly" alternative to solvents and reagents commonly employed in reaction and phase separation processes. Much of this attention stems from CO_2 being nontoxic, odorless, nonflammable, noncorrosive, relatively inexpensive, and widely available. The tunable solvent properties of CO_2 have also attracted interest, as relatively small changes in temperature and pressure often allow for significant changes in viscosity, density, and self-diffusivity.[1] In recent years, dimethyl carbonate (DMC) has been employed as a "green" alternative to conventional methylating and acylating agents primarily because of the fact that it is nontoxic and biodegradable, has a relatively low vapor pressure, and is produced from the industrially clean oxidative acylation of methanol.[2,3] A binary mixture of CO_2 and DMC in both its expanded-liquid[4] and supercritical state provides a hybrid medium that combines the tunable physicochemical properties of pure CO_2 with the liquid solvation properties of pure DMC.

The phase behavior of the CO_2−DMC binary mixture has become a subject of recent study with the proposal of alternative DMC production pathways involving direct synthesis from methanol and CO_2.[5,6] Researchers have also employed the CO_2−DMC binary mixture as a solvent for the tunable synthesis of carbamates from primary aliphatic amines (see Scheme 1).[7−13] In this specific case, the binary mixture functions as both the reaction solvent *and* the reagent, hence eliminating the need for auxiliary materials and additional processing steps. In a separate study, our group reported on the use of the CO_2−DMC binary mixture for the synthesis of nitrogen heterocycles via the in situ conversion of amines to their carbamate derivatives prior to Pictet−Spengler cyclization.[14] We discovered that carbamate yield and selectivity varied appreciably with process operating conditions because of phase-specific partitioning effects, which in turn prompted us to examine the phase behavior of CO_2−DMC binary mixtures in greater detail. To this end, we have measured the mixture critical points and liquid-phase density, component concentration, and volume expansion behavior for the CO_2−DMC binary mixture at temperatures between (310 and 423) K [(37 to 150) °C] and pressures between (1.1 and 14.4) MPa. Knowledge of how these physical properties vary with respect to operating conditions is essential for the successful design, implementation, and commercialization of CO_2-based processes. Mixture critical points, for example, dictate the operating conditions whereby mono- or multiphasic behavior exist—an issue that is paramount when obtaining and interpreting kinetic and thermodynamic data.

Although vapor−liquid equilibrium (VLE) phase composition data for the CO_2−DMC binary mixture have been previously reported,[6,15] a review of the literature revealed that none of the thermodynamic properties presented in this work have been previously published. Data herein were well-correlated using a traditional approach involving a cubic equation of state (EOS) coupled with binary interaction parameters, where we anticipated that the Redlich−Kwong (RK)−Aspen EOS would perform well. Empirical engineering correlations capable of predicting VLE properties for this binary mixture were also developed and might be useful for predicting *PTxy* data which are currently unavailable. Extrapolation of these methods to experimental conditions and chemical systems not examined in this work has yet to be tested. Nonetheless, the experimental and modeling procedures outlined herein may be adapted to other carbon dioxide−liquid binary mixtures and used to facilitate the design of CO_2-based reaction and phase separation processes.

Experimental Section

Chemicals. Supercritical extraction-grade CO_2 of mass fraction purity 0.999999 supplied by Airgas and high-performance liquid chromatography (HPLC)-grade anhydrous DMC of mass fraction purity > 0.999 supplied by Sigma-Aldrich were used without further purification for all experiments. Argon (Ar) of mass fraction purity 0.999999 supplied by Airgas was used without further purification as an inert purge prior to VLE measurements.

Apparatuses. Three independent experimental systems were used in this study, including a: (1) mixture critical point apparatus, (2) liquid-phase density and component concentration apparatus, and (3) liquid-phase volume expansion apparatus.

* Author to whom correspondence should be addressed. E-mail: testerel@mit.edu. Tel.: 617-253-7090. Fax: 617-258-5042.

10.1021/je900948n
Published on Web 03/17/2010

Scheme 1. Synthesis of Carbamates from the Reaction of Amines with CO_2 and DMC

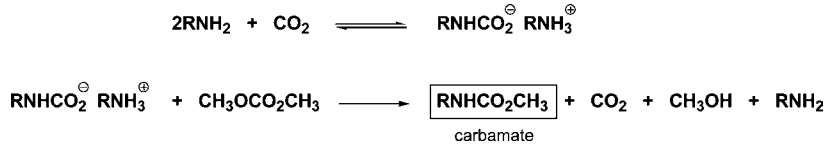

All three systems were serviced by a high-pressure manifold; pressurized CO_2 was delivered by way of a metering pump, while Ar was supplied directly from a pressurized cylinder via a gas regulator. Detailed piping and instrumentation diagrams for the experimental apparatuses are provided in the Supporting Information.

Mixture Critical Point Apparatus. The mixture critical point apparatus consisted of a 25 cm^3 (nominal) stainless steel view cell that allowed visual access via two coaxial sapphire window assemblies. With fittings, the actual vessel volume was approximately 32 cm^3. Mixing was achieved by a magnetic stir bar driven externally by a stir plate. The vessel was connected to a manual pressure generator, which was essentially a crank-driven variable-volume cylindrical chamber. Turning the generator crank counterclockwise, for example, moved an internal piston away from the cell, thereby increasing the apparatus volume by making more of the chamber volume accessible. The temperature was measured using a J-type dual-element thermocouple (accuracy ± 0.1 K) connected to both a local controller and a data acquisition (DAQ) system. Temperature set points were attained within ± 0.5 K by interfacing the controller with a variable autotransformer and insulated heating tape wrapped tightly around the exterior cell wall. Cell pressure was measured by a digital pressure gauge that was accurate to ± 0.1 % of the reading.

Liquid-Phase Density and Component Concentration Apparatus. The liquid-phase density and component concentration apparatus utilized a 104 cm^3 (nominal) stainless steel vessel that similarly afforded visual access via two coaxial sapphire windows. The vessel was equipped with a magnetically coupled stirrer containing two turbine impellers that were positioned to provide phase-specific mixing. Temperature was measured using a thermocouple that was identical to that of the mixture critical point cell. Pressure was monitored by a pressure transducer (uncertainty of ± 0.35 MPa) that was interfaced with a process control unit. The controller achieved desired set-point temperatures within ± 0.2 K by manipulating the electrical power fed to four heating cartridges located within the vessel walls. A metering pump was used to recirculate fluids between phases at a rate of 0.13 $cm^3 \cdot s^{-1}$. Depending on the positions of valves mounted at the pump inlet and outlet, it was possible to recirculate (or sample) a CO_2-rich phase into a liquid phase and vice versa. Phase-specific samples were procured by manipulating a six-way HPLC valve equipped with a 0.100 cm^3 (nominal) sample loop. The actual sample loop volume was 0.104 cm^3, which was determined by the method of standard solutions described by Bezanehtak and co-workers.[16] To ensure that sampling was representative of the vessel contents, all tubing and fittings were wrapped tightly with insulated heating tape and maintained at the vessel temperature within ± 0.5 K via a thermocouple and control logic identical to that of the mixture critical point apparatus. The total working volume of the apparatus was approximately 150 cm^3.

Liquid-Phase Volume Expansion Apparatus. The liquid-phase volume expansion apparatus consisted of a stainless steel/borosilicate glass sight gauge cell with a working volume of 124 cm^3. Because of the relatively large chamber length of the cell, the temperature was measured at both the top and the bottom sections using thermocouples and controllers identical to those of the mixture critical point apparatus. Temperature set points were identical for both portions of the cell and attained within ± 0.5 K by interfacing the controllers with variable autotransformers and a series of strip heaters that were mounted against the external cell walls. Cell pressure was monitored by a pressure transducer that was calibrated against a highly accurate pressure gauge (accuracy ± 0.1 % of reading). Volume measurements were obtained from a liquid-level scale that was readable in 1.6 mm increments and calibrated using 0.50 cm^3 water aliquots from a buret. To ensure phase equilibrium, the metering pump used for the mixture critical point apparatus was used with this apparatus to recirculate the CO_2-rich phase as fine droplets into the liquid phase at a rate of 0.13 $cm^3 \cdot s^{-1}$. All tubing and fittings within the recirculation loop were wrapped tightly with insulated heating tape and maintained at the cell temperature (within ± 0.5 K) using thermocouples and controllers that were identical to the cell temperature control system.

Safety Considerations. Phase behavior measurements at elevated pressure should be carried out only by individuals familiar with the manufacturer's instructions and specifications for the equipment. As a precaution, all experimental apparatuses were operated within a ventilated, thick-walled, shatter-proof enclosure, and pressure relief devices were installed on all high-pressure equipment.

Experimental Procedure. DMC was added as a liquid to all cells by using a syringe. The equipment was then purged with Ar and evacuated prior to the addition of CO_2. Each system was considered equilibrated when the system pressure and temperature fluctuated no more than ± 0.1 MPa and 0.5 K, respectively, and there was no measurable change in the volume of phases present for at least 0.25 h.

Mixture Critical Point Measurements. In a typical experiment, 10 mL of DMC was added to the cell and heated to a desired temperature. CO_2 was added to the cell isothermally, and the pressure was increased until the phase behavior of the initially two-phase mixture became monophasic. After equilibrating, the volume of the cell was increased (and hence the pressure decreased) by slowly adjusting the position of the pressure generator crank. The pressure corresponding to the onset of vapor−liquid phase segregation, commonly referred to as the cloud point, was recorded as the mixture critical pressure ($P_{c,mix}$) at the given experimental temperature. Mixture critical points were reproducible to within 2 % of the reported value.

Liquid-Phase Density and Component Concentration Measurements. Twenty-five cm^3 of DMC was added to the vessel and heated to a desired temperature. CO_2 was then added to the cell, the pressure adjusted to a desired value, and circulation initiated. Following equilibration, a liquid-phase sample was procured in the sample loop. Explained in greater detail in the Supporting Information, liquid-phase CO_2 molar concentration was determined by measuring the volume of fluid that was displaced after directing the sample to an inverted buret filled with CO_2-saturated water:

$$c^{L}_{CO_2} = \frac{n^{L}_{CO_2}}{V^{L}_{S}} \quad (1)$$

where c is the molar concentration, n is the number of moles and is proportional to the displaced volume, V_s is the total volume of the liquid sample, and the superscript L denotes a liquid-phase property. Liquid-phase density was calculated from the molar concentration using eq 2:

$$\rho^{L} = \frac{c^{L}_{CO_2}}{x_{CO_2}} \sum_i x_i M_i \quad (2)$$

where ρ is the mass density, x is the liquid-phase mole fraction, M is the molar mass, and the subscript i is the component index.

The concentration of DMC was determined by combining eqs 1 and 2 and noting that $\sum_i x_i = 1$:

$$c^{L}_{DMC} = \frac{1 - x_{CO_2}}{x_{CO_2}} c^{L}_{CO_2} \quad (3)$$

Liquid-phase density and component concentration data were reproducible to within 2 % of their reported values.

Liquid-Phase Volume Expansion Measurements. Approximately 15 cm^3 of DMC was added to the cell and heated to a desired temperature. The actual volume of the initial DMC charge was determined from the liquid level calibration curve. CO_2 was added to the cell, pressure adjusted to a desired value, and circulation initiated. After equilibrating, circulation was terminated, and the volume of the expanded liquid phase was determined as mentioned above.

Liquid-phase volume expansion was calculated using eq 4:

$$(\Delta V/V_0)^{L} = \left[\frac{V^{L}(T,P) - V^{L}_{0}(T, P^{V}_{DMC})}{V^{L}_{0}(T, P^{V}_{DMC})}\right] \cdot 100 \quad (4)$$

where V is the total volume of the liquid phase at the experimental temperature and pressure, V_0 is the total volume of pure DMC at the experimental temperature and corresponding vapor pressure (P^{V}_{DMC}), and the superscript V denotes a vapor-phase property. Volume expansion measurements were reproducible to within 3 % of the reported value, with deviations up to 10 % for measurements taken within 1 MPa of mixture critical pressures.

Validation of Experimental Procedures. Prior to our study of the CO_2−DMC binary mixture, we first validated our experimental apparatuses and procedures by benchmarking phase equilibrium data for the well-documented CO_2−toluene binary mixture. Excellent agreement was found between experimental data by this work when compared with mixture critical point data reported by Ziegler and co-workers[17] (see Figure 1), liquid-phase molar CO_2 concentration values calculated via eq 2 from data reported by Park and colleagues[18] (see Figure 2), and liquid-phase volume expansion data reported by Lazzaroni and co-workers[19] (see Figure 3).

Results and Discussion

Data Reduction. Experimental VLE data presented herein were correlated with the RK−Aspen EOS[20] using Aspen Plus 2004 steady state process simulation software.[21] The Aspen Plus graphical user interface provides a convenient and straightforward way of producing VLE predictions without the need for time-intensive manual EOS manipulation and coding. The

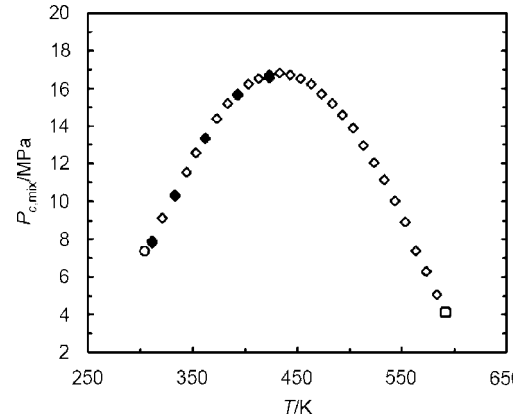

Figure 1. Comparison of experimental mixture critical pressure data for the CO_2−toluene binary mixture: ◆, this work; ◇, Ziegler et al.;[17] ○, P_c of pure CO_2; □, P_c of pure toluene.

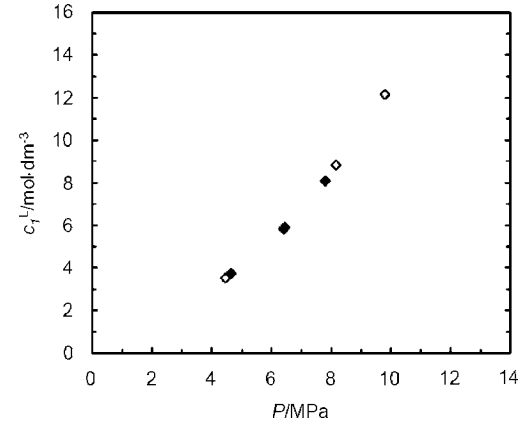

Figure 2. Comparison of experimental liquid-phase concentration data for the CO_2 (1)−toluene (2) binary mixture at 333.2 K: ◆, this work; ◇, calculated via eq 2 from data reported by Park et al.[18]

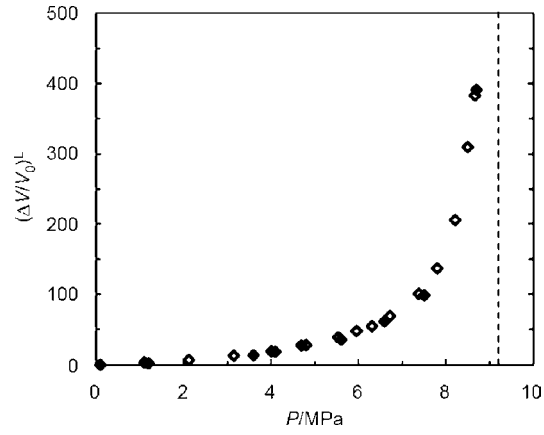

Figure 3. Comparison of experimental liquid-phase volume expansion ($(\Delta V/V_0)^L$) data for the CO_2−toluene binary mixture at 323.2 K: ◆, this work; ◇, Lazzaroni et al.;[19] dashed line indicates the terminus of VLE as indicated by the $P_{c,mix}$ reported by Ziegler et al.[17]

RK−Aspen EOS is particularly attractive for CO_2-based mixtures, as it offers the following: (1) a molecular attraction term that is adjusted to account for components that are in their supercritical state, which enhances agreement with *PVT* data, (2) an empirical polar parameter in the molecular attraction term, which improves the prediction of pure-component vapor pressures of polar species, and (3) mixing rules that contain several temperature-dependent binary interaction parameters, thereby making the equation robust.

The RK−Aspen EOS follows in eq 5:

$$P = \frac{RT}{(V/n) - b} - \frac{a}{(V/n)((V/n) + b)} \quad (5)$$

where P is pressure, R is the universal gas constant, T is temperature, (V/n) is molar volume, a is the molecular attraction term, and b is the molecular covolume term. The RK−Aspen EOS is extended to mixtures by simple mixing rules involving quadratic mole fraction averaging of pure-component values:

$$a = \sum_i \sum_j x_i x_j (a_i a_j)^{0.5} (1 - k_{a_{ij}}) \quad (6)$$

$$b = \sum_i \sum_j x_i x_j \frac{b_i + b_j}{2} (1 - k_{b_{ij}}) \quad (7)$$

where i and j are component indices,and k_{ij} is a binary interaction parameter applied to both the a and b terms that is assumed to vary as a linear function of temperature:

$$k_{a_{ij}} = k^0_{a_{ij}} + k^1_{a_{ij}} \frac{T}{1000} \quad (8)$$

$$k_{b_{ij}} = k^0_{b_{ij}} + k^1_{b_{ij}} \frac{T}{1000} \quad (9)$$

The pure-component molecular attraction (a_i) and covolume terms (b_i) are determined by applying stability criteria ($(\delta P/\delta(V/n))_T = (\delta^2 P/\delta(V/n)^2)_T = 0$) at the critical temperature (T_c) and critical pressure (P_c):

$$a_{c_i} = 0.42747 \frac{R^2 {T_{c_i}}^2}{P_{c_i}} \quad (10)$$

$$b_i = 0.08664 \frac{R T_{c_i}}{P_{c_i}} \quad (11)$$

$$a_i = a_{c_i} \alpha_i \quad (12)$$

where:

$$\alpha_i = [1 + m_i(1 - T_{r_i}^{0.5}) - p_i(1 - T_{r_i})(0.7 - T_{r_i})]^2 \quad (13)$$

$$m_i = 0.48508 + 1.55191\omega_i - 0.15613\omega_i^2 \quad (14)$$

$$T_{r_i} = \frac{T}{T_{c_i}} \quad (15)$$

and α is a factor that adds temperature dependence to the a term and is used to correlate pure-component vapor pressure, m is a constant correlated as a function of the acentric factor (ω), and p_i is an empirical adjustable polar parameter that enhances the accuracy of pure-component vapor pressure for polar species. For nonpolar species such as CO_2, the polar parameter is set to zero. For $T > T_c$, eq 13 is replaced by:

$$\alpha_i = [\exp(c_i(1 - T_{r_i}^{d_i}))]^2 \quad (16)$$

$$c_i = 1 + \frac{m_i}{2} + 0.3p_i \quad (17)$$

$$d_i = 1 - \frac{1}{c_i} \quad (18)$$

Pure-component physical properties for CO_2 and DMC used in the RK−Aspen EOS are listed in Table 1. Binary interaction parameters for the CO_2−DMC system were regressed from a comprehensive experimental VLE data set reported by Im and co-workers[15] from (310 to 340) K [(37 to 67) °C] using the Aspen Plus data regression package. The Britt−Luecke minimization algorithm was used to solve the *PTxy* maximum-likeliness objective function (OF):[22]

$$\mathrm{OF} = \sum_{q=1}^{\mathrm{NDG}} w_q \sum_{z=1}^{\mathrm{NP}} \left[\left(\frac{T_{z,\mathrm{calc}} - T_{z,\mathrm{exp}}}{\sigma_{T_{z,\mathrm{exp}}}} \right)^2 + \left(\frac{P_{z,\mathrm{calc}} - P_{z,\mathrm{exp}}}{\sigma_{P_{z,\mathrm{exp}}}} \right)^2 + \sum_{i=1}^{\mathrm{NC}-1} \left(\frac{x_{i,z,\mathrm{calc}} - x_{i,z,\mathrm{exp}}}{\sigma_{x_{i,z,\mathrm{exp}}}} \right)^2 + \sum_{i=1}^{\mathrm{NC}-1} \left(\frac{y_{i,z,\mathrm{calc}} - y_{i,z,\mathrm{exp}}}{\sigma_{y_{i,z,\mathrm{exp}}}} \right)^2 \right] \quad (19)$$

where NDG is the number of data groups in the regression case, w_q is the weight of data group q ($w_q = 1$ for all groups), NP is the number of datum points in q, NC is the number of components present in q, σ is the experimental error in the specified variable, and the subscripts "exp" and "calc" designate experimental and RK−Aspen EOS-calculated values, respectively. The polar parameter for DMC (p_{DMC}) was determined by minimizing the *PT*-form of the OF from

Table 1. Pure-Component Physical Properties Used with the RK−Aspen EOS[24]

	CO_2[a]	DMC[b]
T_c/K	304.2	557.0
P_c/MPa	7.38	4.80
ω	0.225	0.336

[a] Reported values determined experimentally. [b] Reported values calculated from group contribution methods.

Table 2. Regressed CO_2−DMC Binary Mixture Parameters Used with the RK−Aspen EOS[a]

						AAD[b]/%		
p_{DMC}	$k^0_{a_{ij}}$	$k^1_{a_{ij}}$	$k^0_{b_{ij}}$	$k^1_{b_{ij}}$	T/K	P	x_1	y_1
					310.3	2.9	2.8	0.8
					320.4	2.3	2.2	1.0
0.0388	−0.0402	−0.0263	0.0065	−0.1017	330.3	2.1	1.9	0.7
					340.3	2.4	2.0	0.9
					overall	2.4	2.2	0.8

[a] $p_{CO_2} = 0$. [b] AAD $= (100/N)\sum_1^N |(J_{\mathrm{exp}} - J_{\mathrm{calc}})/J_{\mathrm{exp}}|$, where N is the number of data points and J is the variable of interest.

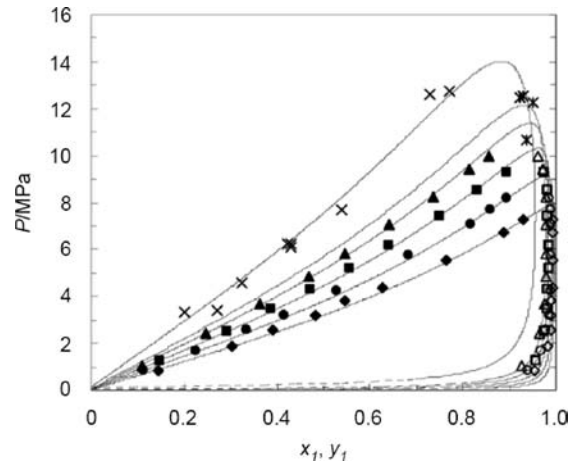

Figure 4. Vapor−liquid equilibria data and modeling for the CO_2 (1)−DMC (2) binary mixture: —, RK−Aspen EOS Px_i and ---, Py_i modeling results from this work. Experimental (Px_i, Py_i) data: ◆ and ◇, $T = 310.3$ K, ref 15; ● and ○, $T = 320.4$ K, ref 15; ■ and □, $T = 330.3$ K, ref 15; ▲ and *, $T = 340.3$ K, ref 15; and × and ∗, $T = 373.6$ K, ref 6.

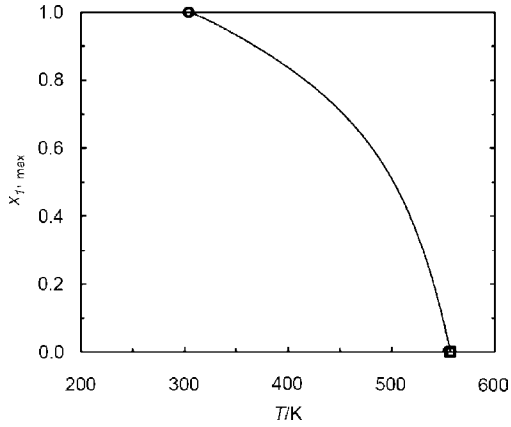

Figure 5. Maximum allowable liquid-phase mole fraction for the CO_2 (1)−DMC (2) binary mixture plotted as a function of temperature: —, RK−Aspen EOS; ○, T_c of pure CO_2; □, T_c of pure DMC.

Table 3. Experimental and RK−Aspen EOS-Calculated Mixture Critical Pressures for the CO_2−DMC Binary Mixture

T/K	$P_{c,mix,exp}$/MPa	$P_{c,mix,calc}$/MPa	AAD/%
310.2	7.7	8.0	3.7
340.2	10.7	11.4	6.4
373.2	12.8	14.0	9.2
403.2	14.1	15.2	7.6
423.2	14.4	15.4	6.6
		overall	6.7

Table 4. Regressed Antoine Parameters (eq 21) Used for the Prediction of Pure-Component Vapor Pressure

	CO_2	DMC
A/MPa	1.071	1.027
B/K	1927	3304
C/K	3.9	41.0
AAD/%	0.22	0.30

pure-component vapor pressure data reported by Rodriguez and co-workers.[23]

Regressed binary interaction parameters and the polar parameter for the RK−Aspen EOS are listed in Table 2. Comparisons between experimental VLE data for the CO_2−DMC binary mixture reported by Im and co-workers[15] and RK−Aspen EOS calculated results by this work are shown in Figure 4. The overall average absolute deviation (AAD) with respect to P_{exp} for a specified x_{exp} is 2.4 % (vs 7 % without the inclusion of the regressed parameter set), which indicates satisfactory agreement between experimental and calculated results. AADs of 2.2 % and 0.8 % with respect to x_{exp} and y_{exp}, respectively, are observed for specified P_{exp}, indicating that predictions are slightly more accurate for vapor-phase compositions. Extrapolation of the RK−Aspen EOS to 373 K results in good agreement with experimental VLE data reported by Camy and co-workers.[6]

The *Pxy* phase envelopes shown in Figure 4 shift leftward and "shrink" with increasing temperature; accordingly, the maximum allowable value of liquid- and vapor-phase CO_2 mole fraction reached at each isotherm decreases with increasing temperature. The maximum allowable liquid-phase CO_2 mole fraction ($x_{CO_2,max}$) as predicted by the RK−Aspen EOS is plotted against temperature in Figure 5 and can be approximated with an AAD of 1.6 % by a cubic polynomial series in temperature T:

$$x_{CO_2,max} = 1.000 - 0.1517\cdot10^{-7}(T/K)^3 + 0.1672\cdot10^{-4}(T/K)^2 - 0.6416\cdot10^{-2}(T/K) \quad (20)$$

Mixture Critical Points. Experimental mixture critical points for the CO_2−DMC binary mixture are given along with a comparison to RK−Aspen EOS calculated values in Table 3. Combining these data with pure-component vapor pressure data affords the *PT* envelope for the CO_2−DMC binary mixture shown in Figure 6. Like many CO_2-liquid binary mixtures, the $P_{c,mix}$ reaches a maximum value as temperature increases from the critical temperature of pure CO_2 to that of pure DMC. Although experimental and calculated mixture critical points show similar behavior with respect to temperature, the RK−Aspen EOS overpredicts $P_{c,mix}$ with an AAD of 6.7 %. Pure-component vapor pressure (P_i^V) curves were generated for CO_2 and DMC by regressing data reported by the National Institute of Standards and Technology (NIST)[25] and Rodriguez and co-workers,[23] respectively, to the form of the Antoine equation:

$$\ln P_i^V = A_i - \frac{B_i}{T - C_i} \quad (21)$$

where A_i, B_i, and C_i are regressed, component-specific parameters and are listed in Table 4. As expected, the RK−Aspen

Table 5. Experimental and RK−Aspen EOS Calculated Liquid-Phase Density and Component Concentration for the CO_2 (1)−DMC (2) Binary Mixture

P		$c^L_{1,exp}$	$c^L_{1,calc}$	$c^L_{2,exp}$	$c^L_{2,calc}$	ρ^L_{exp}	ρ^L_{calc}	AAD
MPa	$x_{1,calc}$	mol·dm^{-3}	mol·dm^{-3}	mol·dm^{-3}	mol·dm^{-3}	kg·m^{-3}	kg·m^{-3}	%
				$T = 310.2$ K				
1.11	0.1818	1.60	2.01	7.19	9.03	718	902	25.7
2.10	0.3411	3.95	4.11	7.63	7.93	861	895	4.0
3.11	0.4896	6.31	6.43	6.58	6.70	870	886	1.9
4.62	0.6775	9.52	9.92	4.53	4.72	827	862	4.2
				$T = 339.7$ K				
1.71	0.1752	1.80	1.85	8.45	8.71	841	866	3.0
3.06	0.3126	3.18	3.53	7.00	7.76	771	855	10.9
4.61	0.4582	5.21	5.57	6.16	6.59	785	838	6.8
6.04	0.5776	7.40	7.44	5.41	5.44	813	817	0.6
7.45	0.6815	9.66	9.15	4.52	4.28	832	788	5.3
8.69	0.7631	10.91	10.43	3.39	3.24	785	751	4.3
				$T = 373.2$ K				
1.85	0.1227	1.35	1.20	9.65	8.58	929	825	11.2
3.82	0.2608	3.00	2.70	8.51	7.66	899	809	10.1
5.97	0.4030	5.15	4.43	7.63	6.56	914	786	14.0
7.84	0.5168	7.09	5.92	6.63	5.54	910	750	16.5
9.65	0.6181	8.02	7.29	4.96	4.50	800	726	9.2
							overall	8.7

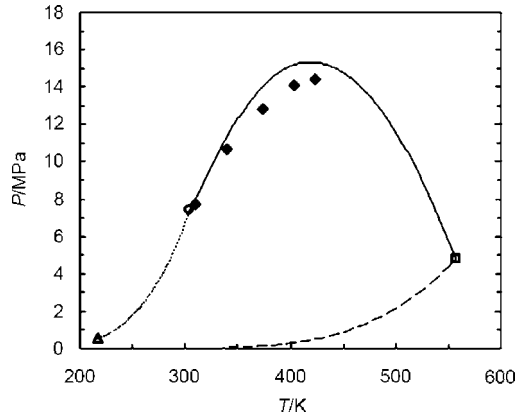

Figure 6. *PT* envelope for the binary CO_2−DMC system: ◆, experimental binary phase envelope and —, as predicted by the RK−Aspen EOS; ---, vapor pressure curve for pure CO_2 and − − −, for pure DMC as predicted by the RK−Aspen EOS; △, triple-point of pure CO_2; ○, P_c of pure CO_2; □, P_c of pure DMC. A continuous binary critical locus was assumed to exist for the unmeasured region between the last experimental datum point and the P_c of pure DMC.

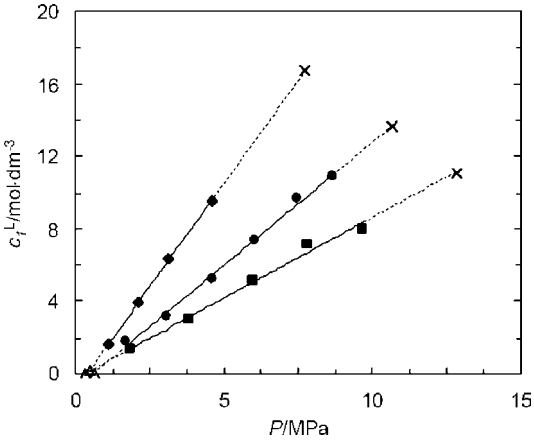

Figure 7. Liquid-phase concentration for the CO_2 (1)−DMC (2) binary mixture plotted as a function of pressure and temperature: ◆, 310.2 K; ●, 339.7 K; ■, 373.2 K; ×, $P_{c,mix}$; —, eq 22; ---, extrapolation using eq 22; △, extrapolated concentration at 1.01 bar for each isotherm.

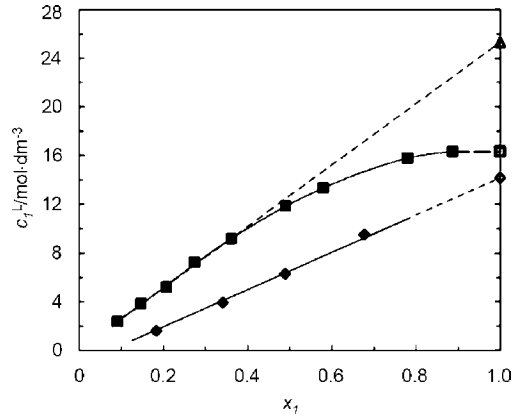

Figure 8. Liquid-phase concentration plotted as a function of liquid-phase mole fraction for the CO_2 (1)−DMC (2) and CO_2 (1)−MeOH (2) binary mixtures: ◆, CO_2−DMC binary mixture by this work at 310.2 K; ■, CO_2−MeOH binary mixture calculated via eq 2 from data reported by Bezanehtak et al.[16] at 308.2 K; ---, extrapolation using eq 23; ▲, extrapolated concentration at $x_1 = 1$ via eq 23 for the CO_2−DMC and △, CO_2-MeOH binary mixtures; □, concentration at $x_1 = 1$ for the CO_2−MeOH binary mixture based on extrapolation of experimental data.

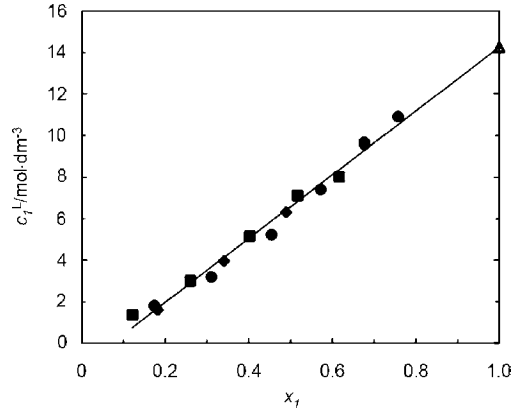

Figure 9. Liquid-phase concentration for the CO_2 (1)−DMC (2) binary mixture plotted as a function of liquid-phase mole fraction: ◆, 310.2 K; ●, 339.7 K; ■, 373.2 K; —, eq 23; ---, extrapolation using eq 23; △, extrapolated concentration at $x_1 = 1$.

EOS accurately predicts the pure-component vapor pressure of both pure CO_2 and DMC, with an AAD of 0.60 % when compared to experimental data.

Liquid-Phase Density and Component Concentration. A comparison between experimental and RK−Aspen EOS-calculated liquid-phase density and component concentration for the CO_2−DMC binary mixture is provided in Table 5. RK−Aspen EOS calculated values deviate from experimental data by an overall AAD of 8.7 %. As shown by Figure 7, liquid-phase CO_2 concentration ($c^L_{CO_2}$) increases with increasing pressure, and at higher temperatures, larger pressures are required to arrive at identical values of $c^L_{CO_2}$ experienced at lower temperature conditions. Liquid-phase DMC concentration (c^L_{DMC}) data exhibit inverse behavior with respect to temperature and pressure. Liquid-phase component concentrations are well-correlated by a linear expression with respect to pressure:

$$c_i^L = \alpha_{c_i^L} P + \beta_{c_i^L} \quad (22)$$

where $\alpha_{c_i^L}$ and $\beta_{c_i^L}$ are regressed, component-specific parameters and are listed in Table 6.

Extrapolation of eq 22 to the $P_{c,mix}$ at each isotherm reveals a maximum possible liquid-phase CO_2 concentration ($c^L_{CO_2,max}$). Liquid-phase component concentrations calculated by the RK−Aspen EOS diverge nonlinearly from eq 22 at pressures within ca. 15 % of the $P_{c,mix}$, resulting in a $c^L_{CO_2,max}$ that is 12 % lower than predicted by eq 22. Experimental deviations in $c^L_{CO_2}$ from linearity are not surprising, as nonlinear behaviors with respect to pressure and composition are often experienced in the vicinity of $P_{c,mix}$ and become more pronounced at higher temperatures (see Figure 4). The CO_2−methanol (MeOH) binary mixture, for example, exhibits a strong deviation in $c^L_{CO_2}$ from linearity with respect to pressure in the vicinity of $P_{c,mix}$ when compared with the CO_2−DMC binary mixture (see Figure 8).

Interestingly, experimental $c^L_{CO_2}$ data for each isotherm collapse to a single trend (see Figure 9) when plotted as a

Table 6. Regressed Parameters (eq 22) Used for the Prediction of Liquid-Phase Component Concentration for the CO_2 (1)−DMC (2) Binary Mixture

T	α_{c1}^L	β_{c1}^L	AAD	α_{c2}^L	β_{c2}^L	AAD
K	MPa^{-1}	mol·dm^{-3}	%	MPa^{-1}	mol·dm^{-3}	%
310.2	2.267	−0.8329	2.2	−1.238	10.3019	1.3
339.7	1.358	−0.7858	5.0	−0.677	9.3819	3.2
373.2	0.891	−0.2658	3.6	−0.572	10.8103	3.3
		overall	3.6		overall	2.6

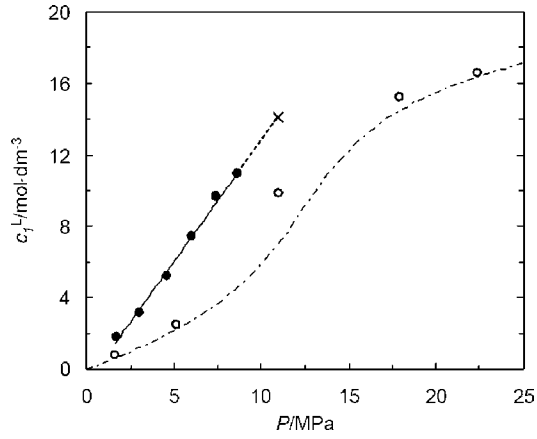

Figure 10. Liquid-phase concentration, ●, for the CO_2 (1)−DMC (2) binary mixture and molar density, ○, of pure CO_2 plotted as a function of pressure at $T = 339.7$ K: —, eq 23; ---, extrapolation using eq 23; ×, $P_{c,mix}$ for the CO_2−DMC mixture; -−-, NIST correlation[25] for pure CO_2.

function of x_{CO_2} and are correlated with an AAD of 8.1 % by:

$$c^L_{CO_2} = 15.2756x_{CO_2} - 1.0910 \quad (23)$$

With x_{CO_2} known as a function of pressure up to the $P_{c,mix}$ from the RK−Aspen EOS, eq 23 provides a relatively simple and straightforward way to estimate the $c^L_{CO_2}$ for the CO_2−DMC binary mixture at any *PT* condition. Extrapolation of eq 23 to $x_{CO_2} = 0$ reveals a nonzero intercept, which is indicative of the experimental error in $c^L_{CO_2}$ data as well as the error in x_{CO_2} predictions by the RK−Aspen EOS. Extrapolation to $x_{CO_2} = 1$ reveals an overall maximum attainable liquid-phase CO_2 concentration for the CO_2−DMC binary mixture of about 14 mol·dm^{-3}. Similar to the trend observed with $x_{CO_2,max}$ (see Figure 5), $c^L_{CO_2,max}$ is largest in the vicinity of the T_c of pure CO_2 and decreases continuously to zero as temperature approaches the T_c of pure DMC. The temperature dependence of $c^L_{CO_2,max}$ can be approximated with an AAD of 2.0 % by combining eqs 20 and 23 to give a cubic polynomial series in temperature of:

$$c^L_{CO_2,max} = -13.74\cdot10^{-7}(T/K)^3 + 15.20\cdot10^{-4}(T/K)^2 - 5.83\cdot10^{-1}(T/K) + 89.82 \quad (24)$$

Pure CO_2 concentration (c_{CO_2}) data were also measured and are compared with $c^L_{CO_2}$ data obtained for the CO_2−DMC binary mixture. As shown by Figure 10, an interesting and often unnoticed property of CO_2−liquid binary mixtures is that the concentration of CO_2 in the expanded-liquid phase in the lower-pressure regime is often larger than the concentration of pure CO_2 when compared at the same *T* and *P*. Accordingly, CO_2-expanded liquids may be desirable over pure CO_2 for synthetic transformations with reaction rate and selectivity dependencies on the molar concentration of CO_2 (e.g., see Scheme 1).

Liquid-Phase Volume Expansion. Liquid-phase volume expansion data for the CO_2−DMC binary mixture are presented in Table 7 along with RK−Aspen EOS calculations. At a fixed temperature, liquid-phase volume expansion increases exponentially up to several hundred percent with increasing pressure. As shown by Figure 11, larger pressures are required to arrive at identical values of $(\Delta V/V_0)^L$ that are obtained at lower temperatures. Data are well-correlated by a series of two exponentials:

$$(\Delta V/V_0)^L = \alpha_{(\Delta V/V_0)^L} \exp(\beta_{(\Delta V/V_0)^L} P) + \chi_{(\Delta V/V_0)^L} \exp(\delta_{(\Delta V/V_0)^L} P) \quad (25)$$

where $\alpha_{(\Delta V/V_0)^L}$, $\beta_{(\Delta V/V_0)^L}$, $\chi_{(\Delta V/V_0)^L}$, and $\delta_{(\Delta V/V_0)^L}$ are regressed parameters and are listed in Table 8.

Compared to experimental data, RK−Aspen EOS calculated $(\Delta V/V_0)^L$ differ by an AAD of 21.8 %, with deviations becoming more pronounced at higher temperatures. Large deviations are not surprising, as the RK−Aspen EOS fails to accurately predict liquid-phase density for both the CO_2−DMC binary mixture (see Table 5) and pure DMC (the RK−Aspen EOS underpredicts liquid-phase density of saturated DMC by 12 % to 30 %).

Table 7. Comparison of Experimental and RK−Aspen EOS Calculated Liquid-Phase Volume Expansion for the CO_2 (1)−DMC (2) Binary Mixture

P		$(\Delta V/V_0)^L_{exp}$	$(\Delta V/V_0)^L_{calc}$	AAD	*P*		$(\Delta V/V_0)^L_{exp}$	$(\Delta V/V_0)^L_{calc}$	AAD
MPa	$x_{1,calc}$	%	%	%	MPa	$x_{1,calc}$	%	%	%
				$T = 310.3$ K					
1.17	0.1913	12	12	0.2	5.41	0.7614	140	177	25.8
1.89	0.3080	23	23	2.1	6.42	0.8576	337	353	4.7
2.46	0.3966	25	34	38.3	6.85	0.8958	557		
3.04	0.4799	39	48	24.2	7.00	0.9093	606	626	3.4
3.54	0.5478	51	64	24.6	7.14	0.9221	716	757	5.7
4.41	0.6535	76	101	33.2	7.29	0.9339	736		
				$T = 340.2$ K					
2.75	0.2819	26	22	17.0	7.79	0.7046	118	144	21.9
3.18	0.3247	33	27	17.6	8.51	0.7475	164		
3.54	0.3596	27	31	15.0	8.65	0.7608	168	198	17.4
3.98	0.4004	33	37	13.2	9.37	0.8054	230	266	15.8
4.84	0.4782	45	52	15.1	10.38	0.8668	375	451	20.4
5.85	0.5623	61	74	21.4	10.67	0.8798	487		
6.57	0.6178	73	94	29.7	10.96	0.9050	684	723	5.7
7.57	0.6854	113							
				$T = 373.6$ K					
1.70	0.1115	18	8	57.1	10.38	0.6548	92	127	37.9
2.18	0.1452	20	10	49.2	11.53	0.7145	119	175	47.3
4.00	0.2720	32	23	28.8	12.40	0.7597	175	230	31.4
4.26	0.2906	32			13.19	0.8038	204	317	55.6
6.13	0.4118	40	43	8.3	13.62	0.8337	375		
8.08	0.5288	70	71	1.7	14.05	0.9118	843		
9.60	0.6135	103	104	1.0				overall	21.8

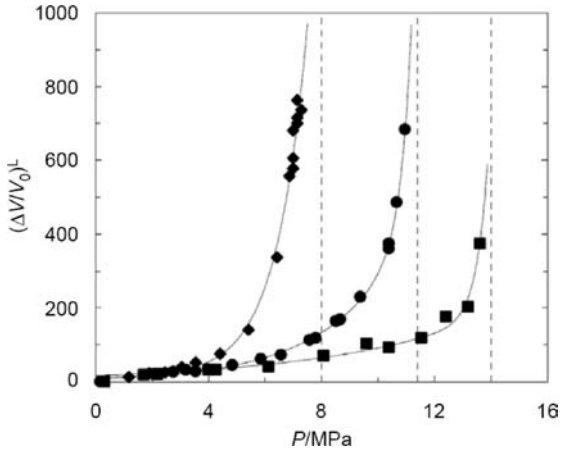

Figure 11. Liquid-phase volume expansion for the CO_2−DMC binary mixture plotted as a function of pressure and temperature: ◆, T = 310.3 K; ●, T = 340.2 K; ■, T = 373.6 K; —, eq 25; and ---, terminus of VLE as indicated by $P_{c,mix}$.

Table 8. Regressed Parameters Used with Equation 25 for the Prediction of Liquid-Phase Volume Expansion for the CO_2−DMC Binary Mixture

T	$\alpha_{(\Delta V/V_0)^L}\cdot 10$	$\beta_{(\Delta V/V_0)^L}\cdot 10$	$\chi_{(\Delta V/V_0)^L}$	$\delta_{(\Delta V/V_0)^L}\cdot 10$	AAD
K	%	MPa^{-1}	%	MPa^{-1}	%
310.2	9.257	9.239	10.39	1.159	9.9
340.2	0.000	28.41	7.47	3.605	5.8
373.6	0.000	25.79	16.33	1.717	9.9
				overall	8.5

Deviations in volume-related properties such as these are often mitigated with the incorporation of volume translation corrections to the cubic EOS.[26]

When plotted as a function of x_{CO_2}, experimental $(\Delta V/V_0)^L$ data sets for each isotherm collapse to a single trend (see Figure 12) that is correlated with an AAD of 12.1 % by:

$$(\Delta V/V_0)^L = 13.530 \exp(2.07x_{CO_2}) + 2.504\cdot 10^{-2} \exp(11.00x_{CO_2}) \quad (26)$$

As in the case of $c^L_{CO_2,max}$, the maximum possible liquid-phase volume expansion obtained for each isotherm is achieved in the vicinity of the $P_{c,mix}$, assumes an overall maximum near the T_c of pure CO_2, and decreases continuously to zero as temperature approaches the T_c of pure DMC.

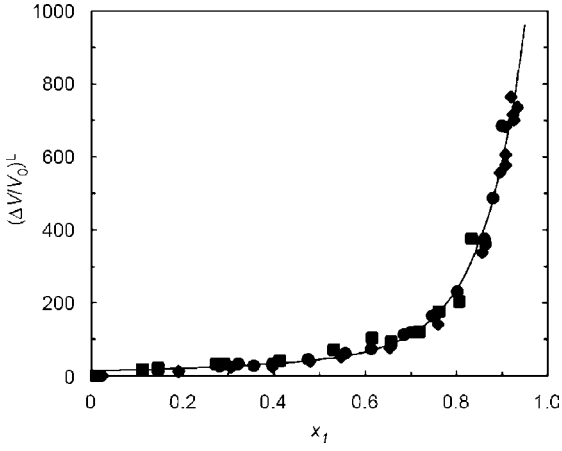

Figure 12. Liquid-phase volume expansion for the CO_2 (1)−DMC (2) binary mixture plotted as a function of liquid-phase mole fraction: ◆, T = 310.3 K; ●, T = 340.2 K; ■, T = 373.6 K; —, eq 26.

Conclusions

Mixture critical points and liquid-phase density, component concentration, and volume expansion were measured for the carbon dioxide−DMC binary mixture at temperatures between (310 and 423) K [(37 to 150) °C] and pressures between (1 and 14.4) MPa. Coupled with regressed binary interaction parameters, the RK−Aspen EOS was capable of reproducing experimental VLE data with an AAD of 2.4 %.

Mixture critical pressure data for the CO_2−DMC binary mixture varied nonlinearly with respect to temperature and were overpredicted by 6.7 % on average by the RK−Aspen EOS. Liquid-phase density and component concentration data were found to deviate from RK−Aspen predictions by an overall AAD of 8.7 %. At a fixed temperature, the liquid-phase CO_2 concentration increased linearly with increasing pressure, attaining a maximum value in the vicinity of the mixture critical pressure. The maximum attainable liquid-phase CO_2 concentration decreased nonlinearly with increasing temperature, assuming a maximum overall value of about 14 $mol\cdot dm^{-3}$ in the vicinity of the critical temperature of CO_2. The liquid-phase component concentration collapsed onto a single, linear trend when plotted as a function of liquid-phase mole fraction. Interestingly, liquid-phase CO_2 concentrations were in some cases up to four times larger for the CO_2−DMC binary mixture when compared with pure CO_2 at the same temperature and pressure. Accordingly, CO_2-expanded liquids may be desirable over pure CO_2 for synthetic transformations with reaction rate and selectivity dependencies on the molar concentration of CO_2. Liquid-phase volume expansion data deviated from the RK−Aspen EOS by an overall AAD of 21.8 % because of the general inability of untranslated cubic EOS's to accurately predict liquid-phase density.[26] At fixed temperature, liquid-phase volume expansion increased exponentially with increasing pressure. When plotted as a function of liquid-phase mole fraction, volume expansion data assumed the functionality of a single, exponential trend.

With the ability to generate VLE data from the RK−Aspen EOS, the empirical trending of thermodynamic properties with liquid-phase mole fraction affords a relatively simple and straightforward way of property estimation for the CO_2−DMC binary mixture. Extrapolation of these methods to experimental conditions and chemical systems not examined in this work has yet to be tested. Nonetheless, the experimental and modeling procedures outlined herein may be adapted to other carbon dioxide−liquid binary mixtures and used to facilitate the design of CO_2-based reaction and phase separation processes.

Acknowledgment

We would like to thank Professors Rick Danheiser, Andrew Holmes, Kathleen Swallow, Bill Green, and their respective research groups, as well as Tester group members Scott Paap, Kurt Frey, Chad Augustine, and Michael Timko, and for helpful discussions pertaining to equipment design, analytical methods, and data modeling.

Supporting Information Available:

Detailed piping and instrumentation diagrams for experimental equipment used in this study along with a derivation of liquid-phase density and component concentration data from inverted buret measurements are provided. This material is available free of charge via the Internet at http://pubs.acs.org.

Literature Cited

(1) Beckman, E. Supercritical and Near-Critical CO_2 in Green Chemical Synthesis and Processing. *J. Supercrit. Fluids* **2004**, *28*, 121–191.

(2) Selva, M.; Perosa, A. Green Chemistry Metrics: A Comparative Evaluation of Dimethyl Carbonate, Methyl Iodide, Dimethyl Sulfate and Methanol as Methylating Agents. *Green Chem.* **2008**, *10*, 457–464.
(3) Pacheco, M. A.; Marshall, C. L. Review of Dimethyl Carbonate Manufacture and Its Characteristics as a Fuel Additive. *Energy Fuels* **1997**, *11*, 2–29.
(4) For a comprehensive review on the properties of gas-expanded liquids, see: Jessop, P. G.; Subramaniam, B. Gas-Expanded Liquids. *Chem. Rev.* **2007**, *107*, 2666–2694.
(5) Piñero, R.; Garcia, J.; Sokolova, M.; Cocero, M. J. Modelling of the Phase Behavior for the Direct Synthesis of Dimethyl Carbonate from CO_2 and Methanol at Supercritical or Near Critical Conditions. *J. Chem. Thermodyn.* **2007**, *39*, 536–549.
(6) Camy, S.; Pic, J.-S.; Badens, E.; Condoret, J.-S. Fluid Phase Equilibria of the Reacting Mixture in the Dimethyl Carbonate Synthesis from Supercritical CO_2. *J. Supercrit. Fluids* **2003**, *25*, 19–32.
(7) Tundo, P.; Perosa, A.; Zecchini, F., Eds. *Methods and Reagents for Green Chemistry. An Introduction*; Wiley: New York, 2007.
(8) Selva, M.; Perosa, A.; Tundo, P.; Brunelli, D. Selective *N*,*N*-Dimethylation of Primary Aromatic Amines with Methyl Alkyl Carbonates in the Presence of Phosphonium Salts. *J. Org. Chem.* **2006**, *71*, 5770–5773.
(9) Selva, M.; Tundo, P.; Perosa, A.; Dall'Acqua, F. Synthesis of Methyl Carbamates from Primary Aliphatic Amines and Dimethyl Carbonate in Supercritical CO_2: Effects of Pressure and Cosolvents and Chemoselectivity. *J. Org. Chem.* **2005**, *70*, 2771–2777.
(10) Tundo, P.; Bressanello, S.; Loris, A.; Sathicq, G. Direct Synthesis of N-Methylurethanes from Primary Amines with Dimethyl Carbonate. *Pure Appl. Chem.* **2005**, *77*, 1719–1725.
(11) Selva, M.; Tundo, P.; Perosa, A. The Synthesis of Alkyl Carbamates from Primary Aliphatic Amines and Dialkyl Carbonates in Supercritical Carbon Dioxide. *Tetrahedron Lett.* **2002**, *43*, 1217–1219.
(12) Tundo, P.; Selva, M. The Chemistry of Dimethyl Carbonate. *Acc. Chem. Res.* **2002**, *35*, 706–716.
(13) Aresta, M.; Quaranta, E. Mechanistic Studies on the role of Carbon Dioxide in the Synthesis of Methylcarbamates from Amines and Dimethylcarbonate in the Presence of CO_2. *Tetrahedron* **1991**, *47*, 9489–9502.
(14) Dunetz, J. R.; Ciccolini, R. P.; Fröling, M.; Papp, S. M.; Allen, A. J.; Holmes, A. B.; Tester, J. W.; Danheiser, R. L. Pictet-Spengler Reactions in Multiphasic Supercritical Carbon Dioxide/CO_2-Expanded Liquid Media.In Situ Generation of Carbamates as a Strategy for Reactions of Amines in Supercritical Carbon Dioxide. *Chem. Commun.* **2005**, *35*, 4465–4467.
(15) Im, J.; Kim, M.; Lee, J.; Kim, H. Vapor-Liquid Equilibria of Binary Carbon Dioxide + Alkyl Carbonate Mixture Systems. *J. Chem. Eng. Data* **2004**, *49*, 243–245.
(16) Bezanehtak, K.; Combes, G. B.; Dehghani, F.; Foster, N. R. Vapor-Liquid Equilibrium for Binary Systems of Carbon Dioxide + Methanol, Hydrogen + Methanol, and Hydrogen + Carbon Dioxide. *J. Chem. Eng. Data* **2002**, *47*, 161–168.
(17) Ziegler, J. W.; Dorsey, J. G.; Chester, T. L.; Innis, D. P. Estimation of Liquid-Vapor Critical Loci for CO_2-Solvent Mixtures Using a Peak-Shape Method. *Anal. Chem.* **1995**, *67*, 456–461.
(18) Park, S.-D.; Kim, C.-H.; Choi, C.-S. Phase Equilibria and Mixture Densities Measurements of Carbon Dioxde-Toluene System under High Pressure. *Hwahak Konghak* **1990**, *28*, 438–443.
(19) Lazzaroni, M. J.; Bush, D.; Brown, J. S.; Eckert, C. A. High-Pressure Vapor-Liquid Equilibria of Some Carbon Dioxide + Organic Binary Systems. *J. Chem. Eng. Data* **2005**, *50*, 60–65.
(20) Mathias, P. M. A Versatile Phase Equilibrium Equation of State. *Ind. Eng. Chem. Process Des. Dev.* **1983**, *22*, 385–391.
(21) *Aspen Plus version 2004.1*; Aspen Technology, Inc.: Burlington, MA, 2004.
(22) Britt, H. I.; Luecke, R. H. The Estimation of Parameters in Nonlinear, Implicit Models. *Technomet.* **1973**, *15*, 233–247.
(23) Rodriguez, A.; Canosa, J.; Dominguez, A.; Tojo, J. Isobaric Vapour-Liquid Equilibria of Dimethyl Carbonate with Alkanes and Cyclohexane at 101.3 kPa. *Fluid Phase Equilib.* **2002**, *198*, 95–109.
(24) Poling, B. E.; Prausnitz, J. M.; O'Connell, J. P. *The Properties of Gases and Liquids*, 5th ed.; McGraw-Hill: New York, 2001.
(25) *National Institute of Standards and Technology (NIST) Chemistry WebBook*, Standard Reference Database Number 69; NIST: Gaithersburg, MD, 2005; http://webbook.nist.gov/chemistry.
(26) Frey, K.; Augustine, C.; Ciccolini, R. P.; Paap, S.; Modell, M.; Tester, J. W. Volume Translation in Equations of State as a Means of Accurate Property Estimation. *Fluid Phase Equilib.* **2007**, *260*, 316–325.

Received for review November 4, 2009. Accepted February 9, 2010. We would like to thank the United States Environmental Protection Agency (EPA) Science to Achieve Results (STAR) Fellowship Program, the Martin Family Foundation Fellowship for Sustainability, and the MIT Undergraduate Research Opportunity Program (UROP) for generous financial support.

JE900948N